Published in final edited form as:
J Biomech Eng. 2008 December ; 130(6): 061018. doi:10.1115/1.2978990.

On Modeling Morphogenesis of the Looping Heart Following Mechanical Perturbations

Ashok Ramasubramanian, **Nandan L. Nerurkar**, **Kate H. Achtien**, **Benjamin A. Filas**, **Dmitry A. Voronov**, and **Larry A. Taber***
Department of Biomedical Engineering, Washington University in St. Louis, St. Louis, MO 63130

Abstract

Looping is a crucial early phase during heart development, as the initially straight heart tube (HT) deforms into a curved tube to lay out the basic plan of the mature heart. This paper focuses on the first phase of looping, called c-looping, when the HT bends ventrally and twists dextrally (rightward) to create a c-shaped tube. Previous research has shown that bending is an intrinsic process, while dextral torsion is likely caused by external forces acting on the heart. However, the specific mechanisms that drive and regulate looping are not yet completely understood. Here, we present new experimental data and finite element models to help define these mechanisms for the torsional component of c-looping. First, with regions of growth and contraction specified according to experiments on chick embryos, a three-dimensional model exhibits morphogenetic deformation consistent with observations for normal looping. Next, the model is tested further using experiments in which looping is perturbed by removing structures that exert forces on the heart — a membrane (splanchnopleure, SPL) that presses against the ventral surface of the heart and the left and right primitive atria. In all cases, the model predicts the correct qualitative behavior. Finally, a two-dimensional model of the HT cross section is used to study a feedback mechanism for stress-based regulation of looping. The model is tested using experiments in which the SPL is removed before, during, and after c-looping. In each simulation, the model predicts the correct response. Hence, these models provide new insight into the mechanical mechanisms that drive and regulate cardiac looping.

Keywords

heart development; chick embryo; finite elements; biomechanics

I. INTRODUCTION

The heart begins life as a single, relatively straight tube consisting of a thin outer layer of myocardium, a relatively thick middle layer of extracellular matrix called cardiac jelly, and a thin inner layer of endocardium (Fig. 1A,A′). Soon after the heart tube (HT) begins to beat, it bends and twists into a c-shaped tube with outer curvature normally directed toward the right side of the embryo. This deformation, termed *c-looping*, represents the first phase of the morphogenetic process of cardiac looping, which creates the basic pattern of the mature heart [1].

Although looping has been studied for nearly a century, the mechanical mechanisms that drive looping are not yet completely understood. Studies have suggested that the bending component of c-looping is generated by coordinated changes in myocardial cell shape, whereas the

*Electronic address: E-mail: lat@wustl.edu; Corresponding author.

torsional (or rotational) component is caused by external loads on the HT [2,3]. Recently, we proposed that torsion is driven primarily by forces exerted on the HT by the primitive atria (omphalomesenteric veins), the conotruncus (outflow tract), and an overlying membrane called the splanchnopleure (SPL) (Fig. 1A,A') [3]. We speculate that the atria initiate rotation by pushing the HT rightward, and the SPL enhances this rotation by pressing against the ventral surface of the heart (Fig. 1).

To test this hypothesis, we previously conducted a series of experiments and developed a finite element model for the first few hours of looping in the chick embryo [3–5]. (Development of the embryonic chick heart parallels that of the human heart; c-looping in the chick takes ace over a 12-hour period, from approximately 36–48 hours of incubation.) In an intriguing experiment, we found that when a stage-10 embryo is incubated with the SPL removed, the heart initially does not twist, consistent with our previous result that suggested a crucial role for the SPL [3]. After approximately six hours, however, the heart slowly twists into its normal rightward position (Fig. 2A,A′,A″). In addition, microindentation tests have revealed that these hearts stiffen abnormally, primarily on the right side, during the same time frame. From these results, we speculated that, when normal SPL loads are removed, the embryonic heart responds by generating an asymmetric cytoskeletal contraction that belatedly pulls the HT rightward, restoring normal looping. We conducted a number of other experiments, all of which appear to support our hypothesis, and a simple computer model demonstrated the feasibility of such a mechanism [5].

The SPL-removal experiment suggests that the early embryonic heart can adapt to perturbations in normal morphogenetic loads. Because such adaptation is crucial for minimizing congenital heart defects, we herein explore this response in more detail. A more complete computational model for the looping heart is presented, and we describe new experiments that are used to test the validity of the model, as well as our looping hypothesis. Moreover, because mechanical feedback is likely involved in this behavior, a morphomechanical law is proposed for cardiac morphogenesis and tested by comparing computational and experimental results. In general, these new data support our hypothesis and provide new insight into the biomechanical processes that drive and regulate looping.

II. EXPERIMENTAL METHODS

A. Embryo preparation and manipulation

Fertile white Leghorn chicken eggs were incubated in a forced draft incubator at 38.5°C and constant humidity. We studied c-looping during stages 10 to 12 of Hamburger and Hamilton [6] (approximately 36 to 48 hours of a 21-day incubation period). Embryos were cultured using our recently developed method that eliminates surface tension by submerging the embryos under a thin layer of fluid [7]. Briefly, a filter paper ring (Whatman #2) was used to remove the embryo and vitelline membrane from the egg. The embryo was then sandwiched using a second filter paper ring and placed ventral side up in a Petri dish containing control media consisting of 89% Dulbecco's modified Eagle's medium (DME), 10% chicken serum, and 1% antibiotics. To keep the embryo submerged, a stainless steel ring was placed on the assembly. The Petri dish was placed in a plastic bag filled with a mixture of 95% O_2 and 5% CO_2, and the sealed bag was put into a culture incubator, where the embryo develops normally under control conditions.

For mechanical perturbations, the splanchnopleure (SPL) was removed using fine glass needles, and the primitive atria were cut using microscissors (Fine Science Tools). Because the SPL regenerates when it is removed, new tissue was dissected away intermittently as needed.

B. Stiffness measurements

Regional mechanical stiffness was measured using a custom-built microindentation device consisting of a piezoelectric motor and a flexible glass beam, as described in [8]. Following Nerurkar et al. [5] and Remond [9], we measured end-diastolic stiffness in intact hearts in the embryo, with access to the heart gained by removing the SPL. Force, computed from the measured beam deflection and stiffness, was plotted as a function of indentation depth, which is defined as the difference between the indenter tip displacement and the displacement of a point on the heart far from the indenter [8]. The diameter of the indenter tip (about 10 to 15 μm) is small compared to that of the heart tube (about 300 μm at stage 11), making highly localized measurements possible. Because the force-displacement curve is nonlinear [10], the regional stiffness (slope of the force-displacement curve) varies with indentation depth. Values are reported here at the representative indentation depth of 15 μm. Unless noted otherwise, all indentation experiments were conducted at room temperature with the heart beat arrested using 0.4 μM verapamil (Sigma).

Stiffness was measured for normal hearts at stage 11 (approximately 42 hr). At least five embryos were indented in each studied region, and the mean and standard error were calculated. Stiffnesses between multiple regions were compared via ANOVA ($p<0.05$ for statistical significance) using SigmaStat software (SPSS Science).

In some experiments, we investigated the effects of cytoskeletal contraction on stiffness. The heart was first tested in control media. Then, to inhibit contractility, 30 μM blebbistatin was added to the media, and the tests were repeated. Blebbistatin is a potent, fast-acting, and highly specific inhibitor of nonmuscle myosin II [11]. These experiments were performed at physiological temperature (37°C) to enhance drug effectiveness. In an earlier study, it was found that neither temperature nor verapamil treatment has a significant effect on end-diastolic stiffness of the embryonic chick heart [5]. Stiffnesses before and after exposure to drugs were compared using paired t-test.

C. Optical coherence tomography

Optical coherence tomography (OCT) is a new imaging technique that provides sub-surface imaging (up to 2 mm deep) of living biological samples with high spatial resolution (10 μm or less) in three dimensions [12]. The system used in these experiments was custom built in the laboratory of Dr. Andrew Rollins at Case Western Reserve University [13]. Briefly, imaging was performed with a laser output of 800 mA at a wavelength of 1310 nm. Cross-sectional images of the embryo were obtained in the horizontal plane as the system scanned the specimen in the vertical direction. At each cross-sectional location (400 total in a 2 mm × 2 mm sampling window), two images were collected and later averaged together in MATLAB (The MathWorks, Inc). The averaged images were cropped, filtered, and reconstructed into volumes using Volocity (Improvision, Inc). Reconstructing the images into volumes enabled the heart to be viewed from any orientation and allowed a more comprehensive understanding of the 3D structure.

D. Tissue labeling

To help visualize heart rotation, small groups of cells in the myocardium were labeled using a 1:10 dilution of the fluorescent dye DiI (Molecular Probes, D-282) in dimethyl sulfoxide. The dye was injected using a pneumatic pump (World Precision Instruments, PV830) via a glass micropipette controlled by a micromanipulator. For embryos starting at stage 10 (36 hr), labels were placed along the ventral midline of the HT. For embryos starting at stages 11 (42 hr) and 12 (48 hr), labels were placed along the outer curvature of the heart. For OCT studies, polystyrene blue-dyed microspheres (Bangs Laboratories) adhered to the myocardium were used instead of fluorescent labels.

III. COMPUTATIONAL METHODS

Computational models for the embryonic heart were used to interpret experimental results and to test hypotheses. The models were analyzed using the finite element software ABAQUS (version 6.4, ABAQUS, Inc.). Tissues are taken as pseudoelastic and slightly compressible, with growth and cytoskeletal contraction included through the user subroutine UMAT, and solution-dependent state variables were used to implement mechanical feedback. The basic ideas are described below; further details can be found in Ramasubramanian and Taber [14].

A. Modeling of morphogenetic mechanisms

A number of basic morphogenetic mechanisms, including cytoskeletal contraction, can be simulated numerically using algorithms for volumetric growth. The approach used in this paper is based on the theory of Rodriguez et al. [15], which assumes the existence of a local stress-free configuration at all times. The theory is well described in the literature [16,17]. Briefly, the total deformation gradient tensor **F** is decomposed into a growth tensor **G** relative to the original zero-stress state and an elastic deformation gradient tensor **K** relative to the current zero-stress state (after growth), i.e.,

$$\mathbf{F}=\mathbf{K}\cdot\mathbf{G}. \tag{1}$$

The field equations for the equilibrium problem are written in terms of **F**. However, because stress is associated only with elastic deformation, the constitutive law is written in terms of **K**. The Cauchy stress tensor is given by [18]

$$\boldsymbol{\sigma}=J^{-1}\mathbf{K}\cdot\frac{\partial w}{\partial \boldsymbol{\varepsilon}}\cdot\mathbf{K}^{T} \tag{2}$$

where J = det **K** and $W(\varepsilon)$ is the strain-energy density function with $\varepsilon = \frac{1}{2}(\mathbf{K}^T\cdot\mathbf{K}-\mathbf{I})$ being the Lagrangian strain tensor for the elastic part of the deformation.

In the looping heart, actin fibers are oriented predominantly in the longitudinal and circumferential directions [19,20]. Assuming that growth and contraction occur primarily along these principal material directions, we take the growth tensor in the orthotropic form

$$\mathbf{G}=\lambda_{gr}\mathbf{e}_r\mathbf{e}_r+\lambda_{g\theta}\mathbf{e}_\theta\mathbf{e}_\theta+\lambda_{gs}\mathbf{e}_s\mathbf{e}_s \tag{3}$$

where the $\mathbf{e}_r$, $\mathbf{e}_\theta$, and $\mathbf{e}_s$ are unit vectors in the local radial, circumferential, and longitudinal directions of the reference configuration, respectively, and the λ_{gi} are corresponding growth stretch ratios. Positive growth is given by $\lambda_{gi} > 1$ with no change in material parameters, while contraction is modeled by taking $\lambda_{gi} < 1$ (negative growth) in the contractile fiber directions, along with an increase in material modulus [*A* in Eq. (7) below].

B. Finite element models

Three finite element models are used in this study. The first model is used to interpret the stiffness measurements, the second is a 3D model for the looping heart with morphogenetic loads specified, and the third is a 2D model for a cross section of the HT in which morphogenetic loads are regulated by mechanical feedback. The material properties for the myocardium and cardiac jelly, taken as uniform throughout in the heart, are given below. The myocardial layer (including the DM) actively grows and contracts, while the jelly remains passive. In these

models, the geometry, boundary conditions, and loads (internal and external) are based on available experimental data, including data presented in this paper.

1. Model for microindentation test—Models were used to help interpret the results from microindentation tests on the primitive atria. It is important to note that the SPL wraps around and is adhered to the lower surfaces of the atria and lies as a relatively flat sheet over the rest of the heart (e.g., see Fig. 4 in [21]). To access the heart, the experiments were conducted with the SPL removed everywhere except where it contacts the atria to avoid damaging the presumptive myocardium.[1] Hence, the lower atrial region was indented with the SPL intact. The models provided a way to estimate the effects of the SPL on measured stiffness.

The atria are idealized as a single curved tube with fixed ends. The centerline radius of curvature and the cross-sectional diameter are both taken as 300 μm (Fig. 3A). Based on OCT images (e.g., Fig. 4B″–D″), the cross-section consists of 15 μm-thick myocardium and 40 μm-thick cardiac jelly enclosing a circular lumen of 95 μm radius. The SPL has the same thickness as the myocardium and forms a sleeve around the lower half of the tube (Fig. 3B). Solid edge (UGS Software) was used to create the geometry, which was meshed using second order tetrahedral elements. To avoid tie conditions, a contiguous mesh was generated using Patran (MSC Software). (This procedure was used to create the geometry for all models.) A higher mesh density was used in the region being indented.

To model indentation, we specified the normal displacement over a small circular region (10 μm diameter) on the surface of the tube (Fig. 3B). The reaction force in the direction of the displacement is available as an output variable in ABAQUS and was obtained via user subroutine URDFIL. To be consistent with the experimental measurements, indentation depth was computed by subtracting the displacement of the point of the surface opposite the indented region from the displacement of the circular region. Stiffness was calculated as the slope of the force-displacement curve at 15-μm indentation depth, as in the experiments.

2. Three-dimensional model for looping—The three-dimensional geometry of the looping heart is idealized from images taken with the SPL removed (e.g., Fig. 4). The HT and primitive atria are modeled as idealized curved tubes consisting of a thin outer layer of myocardium and a relatively thick inner layer of cardiac jelly (similar to the indentation model). When the SPL is removed and the embryo is cultured for six hours from stage 10 to about stage 11, the HT bends ventrally but little torsion occurs [5]. This state (no SPL, no rotation, HT fully bent) forms the initial configuration of the model (Fig. 3B). The outflow tract (conotruncus) is a straight extension of the HT that is attached dorsally to the “embryo” by a strut representing the dorsal mesocardium (DM). The dorsal side of the DM is constrained to move only vertically, and the atria are fixed at their distal ends and oriented at a 45° angle relative to the embryonic plane (see insert in Fig. 3B).

Myocardial growth and contraction are included by ramping the values of the growth stretch ratios from unity at $t = 0$ to specified peak values at the end of the simulation. Following SPL-removal, experiments indicate that abnormal contraction develops along the right side of the heart [5]. Thus, circumferential contraction ($\lambda_{g\theta} = 0.6$) is specified in the right half of the HT and conotruncus. In the atria, experiments suggest that cells move through the upper parts of the atria toward the HT, while the lower parts of the atria contract [3,4,22]. The added cells are simulated by longitudinal growth with $\lambda_{gs} = 1.6$ in the upper half of the atria, while setting $\lambda_{gs} = 0.6$ gives longitudinal contraction in the lower half.

[1]The outer layer of the atria is more properly termed “presumptive myocardium,” because the cells in this layer do not begin to beat until the atria fuse and become part of the HT.

To overcome convergence difficulties, slightly smaller morphogenetic loads are used in the models in which one or both atria are removed. For these models, we set $\lambda_{g\theta} = 0.7$ on the right side of the HT and conotruncus, $\lambda_{gs} = 1.3$ in the upper atrial regions, and $\lambda_{gs} = 0.7$ in the lower atrial regions. Qualitatively, the results are not greatly affected by this modification.

3. Two-dimensional model for looping with feedback—A plane-strain cross-sectional model for the HT is used as a first approximation to explore the role of mechanical feedback during c-looping. In this model, the values of the growth stretch ratios are governed by morphomechanical laws, rather than being prescribed as in the 3D model.

The model consists of a circular layer of myocardium and a characteristic football-shaped lumen (see Fig. 4B″,D″), with cardiac jelly filling the space in between (Fig. 3C). A myocardial extension representing the DM is fixed dorsally to the wall of the foregut, and the SPL is represented by a flat rigid surface. The dimensions are as follows: HT outer diameter = 350 μm, myocardial thickness = 10 μm, cardiac jelly thickness (in the direction of the minor axis of the elliptical lumen) = 140 μm.

This model involves two regions of contact — between the myocardium and the foregut wall and between the myocardium and the SPL (see deformed configurations in Fig. 10). Both of these are modeled as frictionless contact between two surfaces. The myocardium is chosen as the slave surface and either the SPL or the foregut wall becomes the master surface.

Initially, the model is stress free, all growth stretch ratios are set to unity, and all target stresses are set to zero. The simulation begins with a small rightward force applied briefly to the left side of the heart. This force represents the push given by the atria [3]. Then, the myocardium responds on its own according to the morphomechanical laws described below. These laws are integrated in time via finite differences. Further details are given in the Results section.

C. Morphomechanical laws

To include mechanical feedback, we propose mathematical rules that quantify the qualitative observations of Beloussov [23], who postulates that morphogenesis is regulated by tissue stress. From numerous experiments on embryos spanning decades, Beloussov found that perturbations in tissue stress induce an active response that tends to restore the original (target) stress, but usually overshoots (hyper-restores) the stress to the opposite side. For example, if the stress in a certain direction decreases, the tissue actively contracts to increase the stress to a value above the initial value. Similarly, an increased stress induces convergent extension or growth that reduces the stress below its original value. Beloussov [23] calls this idea the Hyper-restoration (HR) Hypothesis.

In an earlier study [14], we proposed a morphomechanical law of the form

$$\mathbf{D}_G = \dot{\mathbf{G}} \cdot \mathbf{G}^{-1} = \mathscr{A} : (\boldsymbol{\sigma} - \boldsymbol{\sigma}^*) \tag{4}$$

where $\mathbf{D}_G$ is the growth-rate tensor, $\mathscr{A}$ is a fourth-order tensor of growth coefficients, $\boldsymbol{\sigma}(t)$ is the current Cauchy stress tensor, and $\boldsymbol{\sigma}^*$ is the target stress tensor, i.e., the stress at morphogenetic equilibrium. For simplicity, the present models consider growth (or contraction) in one direction only (the circumferential direction), leading to the simplified relation

$$D_G = \dot{\lambda}_g(t)/\lambda_g(t) = a(\sigma - \sigma^*) \tag{5}$$

where a is a constant. In [14], the value of the target stress was specified. Here, however, we include hyper-restoration by assuming that σ* evolves according to the equation

$$\dot{\sigma}^* = -b(\sigma - \sigma^*). \tag{6}$$

The minus sign in front of the positive constant b provides the stress overshoot, i.e., when σ > σ*, the target stress σ* decreases, and vice versa. The parameter values are taken as $a = 0.0025$ $(\text{Pa-hr})^{-1}$ and $b = 2\ \text{hr}^{-1}$.

D. Material properties

Material anisotropy of the developing heart has not yet been measured. For simplicity, therefore, we assume that the cardiac jelly and myocardium are nearly incompressible, isotropic, and pseudoelastic materials, with the strain-energy density function for both taken in the form

$$W = \frac{A}{B}\left[e^{B(\bar{I}-3)} - 1\right] + D^{-1}(J-1)^2 \tag{7}$$

where A, B, and D are material coefficients, $J = \det \mathbf{K}$ is the volume ratio, and $\bar{I} = J^{-2/3}\text{tr}(\mathbf{K}^T \cdot \mathbf{K})$ is a modified strain invariant [24]. (Although the material constitutive law is assumed to be isotropic, the models include orthotropic growth and contraction.) Using an equivalent form for W, Zamir and Taber [10] determined A and B for the outer curvature of the stage-12 HT. In the current study, microindentation tests for several other regions revealed that, except for the caudal side of the atria, all regions of the heart have stiffnesses similar to that measured in [10]. Hence, we use the same constants identified in that study ($A = 11$ Pa and $B = 0.49$ for *passive* myocardium; $A = 3.2$ Pa and $B = 0.39$ for cardiac jelly). For nearly incompressible materials, $D \to 0$, and we set $D = 0.01\ \text{Pa}^{-1}$.

To model cytoskeletal contraction in the 3D model, the value of A is changed gradually from its passive value (11 Pa) to its fully active value (33 Pa), while the values of the λ_{gi} decrease from 1.0 to a specified minimum value in the direction of contractile fibers. In the 2D model, the material coefficients are held constant, and the λ_{gi} are determined by integrating the morphomechanical laws.

IV. RESULTS

A. Cardiac morphogenesis following splanchnopleure removal

When the SPL is removed at the onset of looping at stage 10 ($t = 0$), the heart bends ventrally but remains untwisted at stage 11 ($t \cong 6$ hr), and then it twists (rotates) normally by the end of c-looping at stage 12 ($t \cong 12$hr) (Fig. 2A–A″). This result is consistent with the experiments of Nerurkar et al. [5].

When the SPL is removed near the midpoint of c-looping at stage 11, the heart immediately untwists partially (Fig. 2B,B′). However, when the heart is cultured for an additional six hours, rotation is again fully restored (Fig. 2B″). Finally, when the SPL is removed at the end of c-looping (stage 12), there is no noticeable loss of rotation (Fig. 2C,C′), and the heart continues to develop into s-looping [1] upon further culturing (Fig. 2C″).

OCT images indicate that the HT protrudes from the embryonic plane when the compressive force exerted by the SPL is removed (Fig. 4A–D) [21]. This motion pulls the proximal ends of the atria outward so that the atria rotate out of the plane of the embryo. After SPL removal,

the angle of the atria relative to this plane changes from approximately 0° at stage 10 ($t = 0$) to 45° after three hours to 90° after six hours. As shown later, these abnormal changes in morphology may play a role in the late-onset torsion that occurs between stages 11 and 12. Cross-sectional images (Fig. 4A″–D″) illustrate again the behavior observed in Fig. 2A–A″ and allow us to measure the HT rotation angle (see Fig. 4B″).

B. Stiffness measurements

Zamir et al. [8] measured the stiffness of the stage-12 HT. Here, we measured the stiffness of the conotruncus (left and right sides) and primitive atria (upper and lower sides) of *normal* stage-11 hearts. The locations for all measurements are indicated in Fig. 5A.

The stiffnesses of the right and left sides of the conotruncus (RC, LC) and the top side of the left atrium (TLA) were similar to that of the outer curvature (OC), as measured in [8] (Fig. 5B). (In limited experiments, we confirmed that the outer-curvature stiffnesses of stage 11 and 12 hearts are similar.) The stiffness of the bottom side of the atria (BA), however, was significantly higher ($p < 0.001$) than in the other tested regions (Fig. 5B). Exposure to the myosin II inhibitor blebbistatin (30 μM) reduced the lower atrial stiffness by almost 50% (BA, with bleb), suggesting that the higher stiffness is at least partially due to cytoskeletal contraction. This result is consistent with experiments by Voronov et al. [3], who found that exposure to cytochalasin D relaxes the tension on the caudal side of the atria. However, although reduced by blebbistatin, the stiffness in the treated hearts remained about three times higher than that of the other regions.

Further evidence of contraction along the bottom of the atria was obtained by exposing normal hearts (with SPL intact) to blebbistatin. This caused the curvature of the atria along the anterior intestinal portal (AIP) to increase dramatically (compare shape traced by dotted lines in Fig. 6A,A′). Removing atrial contraction from our 3D model yields similar behavior (compare Figs. 6B and B′).

A computational model (Fig. 3) was used to explore the reason why the caudal side of the atria remained significantly stiffer than the other regions when all were rendered passive by exposure to blebbistatin (Fig. 5B). Two possibilities were considered. The first is that the added stiffness is caused by the SPL, which remained attached to the lower atrial region and effectively doubled the thickness of the outer layer. In the model, the presence of the SPL made the bottom about 70% stiffer than the top side of the atria. The second possibility is atrial curvature. This effect was estimated by comparing the stiffnesses at the top and bottom of the model without SPL. (Recall that the top side of the atria had a stiffness similar to that of other regions.) In this case, the bottom is about 30% stiffer, making the cumulative increase in stiffness a factor of approximately 2.2, which is still somewhat smaller than the measured ratio of about 3. The remaining difference could be due to the SPL being inherently stiffer than myocardium or to residual tension in the SPL.

Nerurkar et al. [5] reported that the outer curvature of stage 11 and 12 hearts stiffened in response to the reduced loading caused by SPL removal. For comparison, we also include the stiffness data from these experiments in Fig. 5B (OC, no SPL). Exposure to the Rho-kinase inhibitor Y-27632 reduced the stiffness to normal levels (OC, no SPL, Y), indicating that the increased stiffness is caused by cytoskeletal contraction that is not present when the SPL is intact [5]. That study also found that the abnormal contraction is most prominent on the right side of the HT. (Here, we used the relatively new drug blebbistatin instead of Y-27632, because blebbistatin more specifically targets nonmuscle myosin II [11].)

C. Three-dimensional model for looping without splanchnopleure

As described in the Computational Methods section, we used experimental data as the basis for prescribing regions of growth and contraction in the 3D model (Fig. 7A). At the end of c-looping (without SPL), the model-predicted heart shape matches the experimental shape quite well (compare Fig. 7B with Fig. 2B″). Note that the predicted downward deflection of the atria and the increased curvature of the left atrium agree well with observed behavior. However, while the motions of the labels along the midline of the HT appear to show similar amounts of rotation near the center of the HT, the actual computed rotation angle (29°) is lower than the measured angle (55°).

Perturbed models were analyzed to gauge the relative contributions of the various morphogenetic loads. When contraction is turned off in the HT and conotruncus but left on in the atria, the rotation angle drops to 20° (Fig. 7C). When contraction also is turned off in the atria, so that atrial growth provides the only actively generated force, the angle of rotation decreases further to 15° (Fig. 7D).

Computational modeling also shows that the changes in atria orientation, far from being a curious side effect of SPL removal, may actually help the HT rotate when the SPL is absent. As shown in Fig. 8, the amount of rotation becomes progressively larger as the atria orientation changes from 0° to 45° to 90° relative to the embryonic plane.

Finally, to test the predictive ability of the 3D model, we used a series of experiments that were first reported in [5], in which looping was perturbed by removing the primitive atria at stage 10 (in addition to the SPL). When the left atrium was removed, most hearts (11/15) looped leftward after 12 hr (Fig. 9A,A′). Removing the right atrium resulted in right looping in all hearts (12/12), although heart morphology appeared abnormal, and removing both atria resulted in right looping in all hearts (14/14). Each experiment was simulated using the 3D model. All parameters have the same values during each simulation, with the only difference being the removal of the atria (with the cut ends being traction free). In each case, the morphology produced by the model agrees relatively well with experimental results (Fig. 9). Note that the model predicts correctly the abnormal shape of the remaining atrium, as well as the rightward rotation that occurs when both atria are removed.

D. Two-dimensional model for self-regulation of cardiac rotation

In the 3D model, the values of the morphogenetic forces (growth and contraction) were specified. The experiments suggest, however, that the heart responds actively to the removal of loads exerted by the SPL. This behavior indicates that mechanical feedback is involved. Here, we explore the possibility that the delayed torsion following SPL removal is governed by Beloussov's HR Hypothesis [23].

To test this idea, the 2D model is used to simulate each experiment depicted in Fig. 2, where the SPL was removed at different times during looping (Fig. 10). As discussed in the Computational Methods section, rotation is initiated at stage 10 by a small rightward force temporarily applied to the left side of the HT. Thereafter, the myocardium responds via Eq. (5) and Eq. (6). For convenience, time has been scaled so that the time point for each panel in Fig. 10 corresponds to the panel with the same label in Fig. 2. The three rows in each figure represent SPL removal at stages 10, 11, and 12, respectively.

In the first experiment, the membrane is removed at stage 10 (Fig. 2A and Fig. 10A). After the initial push, the model HT rotates very little during the first six hours, just as in the experiment (Fig. 2A′ and Fig. 10A′). Rotation, however, is fully restored in both the model and experiment during the next six hours (Fig. 2A″ and Fig. 10A″). In the model, rotation stops only because

the HT contacts the wall of the foregut, and the final value of the lumen rotation angle for the model (55°) matches the experimental result (54°).

In the second experiment, the SPL is left intact until stage 11. The SPL is simulated by a frictionless horizontal rigid surface, which gradually pushes the HT downward, forcing it to rotate rightward (Fig. 2B and Fig. 10B). When the membrane is removed at stage 11, the heart springs back as it loses much of its rotation, consistent with the experimental behavior (Fig. 2B′ and Fig. 10B′). Rotation is regained and completed in both the model and experiment during the following six hours (Fig. 2B″ and Fig. 10B″).

Finally, when the SPL is left intact until stage 12 (Fig. 2C and Fig. 10C), the HT essentially remains in its fully rotated position, both experimentally and in the model (Fig. 2C′ and Fig. 10C′). When the embryo, with SPL removed, is cultured for 6 hours from stage 12 to stage 14, s-looping begins [1] and development appears normal (Fig. 2C″). The model, however, only deals with the rotational component of c-looping, which is complete by stage 12; hence, there is no model figure corresponding to Fig. 2C″.

V. DISCUSSION

The cardiac torsion that occurs during looping is one of the first morphological signs of left-right asymmetry in the vertebrate embryo. Looping abnormalities likely underlie some of the cardiac malformations that occur in as many as 1% of liveborn and 10% of stillborn human births [25], and such defects may result in numerous spontaneous abortions during the first trimester [26]. Thus, this problem has received considerable attention for decades. However, while rapid progress is being made in defining the genetic perturbations behind abnormal cardiac morphogenesis [25,27,28], the biomechanical mechanisms that drive and regulate looping are not yet completely understood [1,22].

The impetus for this study stems from our previous experiments that explored the behavior of the looping chick heart following removal of the SPL [5]. Although the SPL normally plays a major role in the torsional component of c-looping [3], those experiments suggest that the heart contains an intrinsic ability to adapt and undergo torsion when this membrane is removed [5]. Such built-in redundancy ensures proper looping even under severely perturbed conditions. Because heart development is vital to the survival of embryo, it is not surprising that such redundancies exist.

In our earlier study of this problem, we found evidence that the observed adaptive torsion is driven by an abnormal cytoskeletal contraction that develops primarily on the right side of the heart and pulls the HT rightward [5]. However, we did not investigate in detail the underlying mechanics to determine whether such a mechanism is fully consistent with physical principles and the observed 3D morphology. Moreover, we did not explore how this response is regulated. The purpose of the present study is to examine these issues using both experimental and computational models.

It is important to recognize that the present work is phenomenological in nature. The simulated mechanisms are based on data regarding cellular activity, but the molecular events that produce this activity are not considered. Moreover, developmental events occurring before and during heart tube formation likely influence looping directionality [25,29,30].

A. Remarks on stiffness measurements

During the last decade, a number of papers have been published on the mechanical properties of embryonic chick hearts during post-looping stages 16 to 31 (2.5 to 7 days) [31–35]. Since an early study of the compressive behavior of the stage-12 heart [36], however, Zamir and

colleagues [8,10] have provided the only measurements of regional stiffness and material properties of the looping heart (also at stage 12). Notably, Zamir et al. [8] found that the right side, left side, and outer curvature of the HT have similar stiffnesses, but the inner curvature is significantly stiffer, possibly due the seam left there by the fused edges of the DM. They speculated that the relatively stiff dorsal side plays a role in the bending component of c-looping.

Here, we measured the stiffness in several other regions of normal stage-11 hearts (developed with SPL intact), including the right and left sides of the conotruncus and the top and bottom of the primitive atria. Taken together, our data show that all regions of the heart at stages 11 and 12 have approximately the same stiffness, with the exception of the lower atrial region, which is significantly stiffer (Fig. 5B). The lower atrial stiffness dropped on exposure to blebbistatin, indicating that the elevated stiffness in this region is at least partially due to cytoskeletal contraction, a finding consistent with previous data [3]. The present 3D model supports the view that this contraction plays a role in the torsional component of c-looping; turning it off in the model results in a significant loss of rotation (Fig. 7C,D).

The indentation problem can be treated as a plate or shallow shell (myocardium) on an elastic foundation (cardiac jelly). Hence, in relatively soft regions of the heart, the deformation is localized to the region near the indenter, and differences in stiffness primarily reflect changes in myocardial thickness or material properties [8,10,37]. However, in the relatively stiff lower atrial region, boundary conditions on the heart may influence the measurements. Our finite element analysis of the indentation experiment accounts for these effects and shows that the relatively high stiffness in this region can be attributed to a combination of contraction, the attached SPL, and longitudinal curvature (Fig. 3). The material properties of the myocardium need not differ from those in other regions of the heart.

B. Remarks on the 3D model (no feedback)

In prior work, we used a 2D finite element model to show that contraction on the right side of the HT and conotruncus can cause the rightward rotation observed following SPL removal [5]. That model, however, does not account for the complex 3D geometry of the embryonic heart and ignores the possible effects of the primitive atria. Here, we developed a more realistic model to test more thoroughly the feasibility of our hypothesis. The model includes circumferential contraction on the right side of the heart (HT, DM, and conotruncus), longitudinal contraction in the lower half of the atria, and longitudinal growth in the upper half of the atria (Fig. 7A). It is important to note that the contraction along the right side of the heart occurs only when the SPL is removed [5]. In this model, the growth stretch ratios for all of these processes are specified a priori.

The deformation of the model, including torsion, is similar qualitatively to that seen experimentally (compare Fig. 7B and Fig. 2B″). The general behavior is consistent with the hypothesis illustrated in Fig. 1, but the model provides more detail about the physical mechanism. First, the forces that the atria exert on the HT arise from two sources. One is the push of cells being added to the upper side of the atria, and the other is an additional push exerted by these same cells as they are pulled toward the heart by contraction of the lower side of the atria. In this model, the left atrium exerts a greater force because it is larger than the right atrium, as generally seen in vivo (e.g., see Fig. 2A). Second, geometric asymmetries convert the atrial forces into forces that cause the HT to rotate, rather than bend, rightward. In particular, the DM serves as a pivot for rotation, and the offset in the atrial cross-sections where they intersect the HT produce a moment that has a torsional component after the heart begins to rotate. The abnormal out-of-plane orientation of the atria when the SPL is removed (Fig. 4) enhances the torsional moment (Fig. 8). Third, when the SPL is removed, all of the forces due to growth and contraction contribute to the observed torsion.

The results from the looping simulations following removal of one or both atria (Fig. 9) seem to provide strong support for our general hypothesis for c-looping, as depicted in Fig. 1. In each simulation, all model parameters have the same values. The only difference is that the left atrium, right atrium, or both atria are removed. In each case, the model yields a shape that agrees reasonably well with that of the experimental heart.

C. Remarks on the 2D model (with feedback)

Feedback likely is involved in the regulation of morphogenesis. In traditional control systems, feedback is used to achieve two goals: (1) *set point regulation*, which involves taking the system response toward a desired value (e.g., cruise control in automobiles) and (2) *disturbance rejection*, which ensures that perturbations do not interfere with set point regulation (e.g., integral control in servo machines). In this paper, we investigate a control law for the rotational component of c-looping, which ensures that (1) the set point (i.e., a fully rotated heart) is reached and (2) rotation is completed even when external disturbances (i.e., SPL removal) are encountered.

The 2D model for looping employs a phenomenological control law based on the HR Hypothesis of Beloussov [23]. The main idea of this hypothesis is that embryonic tissues attempt to maintain a homeostatic stress state by actively changing size and shape (e.g., by growth or contraction) whenever homeostasis is disturbed. The induced response generally overshoots the homeostatic target stress, however, leading to a new response, and so on, until the desired form is created. In this scheme, the perturbation that initiates a morphogenetic process may require genetic activity, but thereafter the cells are autonomous. Recently, we used computational models based on Eq. (5) and Eq. (6) in the present paper to explore the feasibility of the HR Hypothesis for some fundamental problems in morphogenesis [38]. Comparing numerical and experimental results gave mixed agreement, and we concluded that genes must occasionally step in to alter or trigger further cellular activity.

The results from the 2D model show that the HR Hypothesis captures quite well the dynamics of the rotational component of c-looping. The behavior of the model is consistent with the results from three different experiments, where the SPL is removed at stages 10, 11, and 12 (Fig. 2 and Fig. 10). We again emphasize that the same parameters are used for all three simulations. In this model, asymmetric atrial forces supply an initial perturbation that causes the HT to rotate and the DM to bend slightly rightward. The bending produces tension on the convex side and compression on the concave side of the DM, and Eq. (6) makes the initially zero target stresses compressive on the convex side and tensile on the concave side. In response, the concave side contracts and the convex side grows, inducing more bending. This response continues until the HT contacts the wall of the foregut. Interestingly, DM bending stops after the initial perturbation if there is no overshoot, i.e., if b is set to zero in Eq. (6). Thus, stress hyper-restoration is crucial for this model to work.

According to our models, contraction and growth in the DM is necessary for proper rightward rotation, as contraction and growth in the HT does little in itself. Recently, Linask et al. [39] presented evidence supporting this idea. These authors found that the cell proliferation rate is normally higher on the left side than the right side of the DM (and associated splanchnic mesoderm adjacent to the foregut wall). Moreover, inducing hyperplasia on the right side is associated with left looping. They speculate that the added cells on the left side of the DM push the HT rightward, and vice versa, in agreement with the results from our model. Here, we suggest that the observed asymmetric cellular hyperplasia is an HR response to asymmetric stresses caused by external loads.

If the DM is truly needed for proper rotation, then rotation would be compromised if the DM were removed. Experiments confirm that rotation is severely disrupted when the DM is cut

away (results not shown). Also, in an earlier study, we showed, using a 3D model and experimental perturbations, that the DM is critical for the rotational component during the early stages of c-looping [4].

D. Limitations

As mentioned above, element inversion causes convergence issues in the 3D model. The model has approximately 60,000 elements, and the simulation stops even if only one element inverts. This problem is especially acute at the intersection between the HT and the atria. For this reason, some simulations did not proceed to completion. This is the reason that the HT rotation angle (see schematic in Fig. 4B″) at the end of c-looping given by the 3D model (29°, Fig. 7B) is smaller than the measured angle (54°, Fig. 4D″). (Growth on the left side of the DM, which is not included in the 3D model, also may be a factor in the relatively small rotation.) Unfortunately, problems involving large deformation, such as the one considered here, are more susceptible to element inversion. Currently, the limited adaptive remeshing capability found in ABAQUS is insufficient to alleviate this problem.

Because of a lack of experimental data, the values of certain model parameters are just rough estimates. These include the growth law coefficients, growth and contraction stretch ratios, and changes to the material constant A due to contraction. Moreover, it is likely that cardiac jelly is highly viscoelastic. However, viscoelastic material properties for the heart during c-looping also are currently unavailable, and hence these effects are not included.

E. Conclusions

Our models appear to support the notion that c-looping is driven primarily by forces exerted on the heart tube by the SPL and the primitive atria. At the cell level these forces are generated by a combination of cytoskeletal contraction and growth. When these forces are perturbed, the models show that stress hyper-restoration can generate an adaptive mechanism that restores normal looping. Future work is needed to determine whether this concept applies to other developmental processes.

Acknowledgments

This research was supported by grant NIH F32 HL079764 (AR), as well as NIH grants R01 HL64347, R01 GM075200, and R01 HL083393 (LAT). This support is gratefully acknowledged.

References

1. Manner J. Cardiac looping in the chick embryo: A morphological review with special reference to terminological and biomechanical aspects of the looping process. Anat. Rec 2000;259:248–262. [PubMed: 10861359]
2. Latacha KS, Remond MC, Ramasubramanian A, Chen AY, Elson EL, Taber LA. The role of actin polymerization in bending of the early heart tube. Dev. Dyn 2005;233:1272–1286. [PubMed: 15986456]
3. Voronov DA, Alford PW, Xu G, Taber LA. The role of mechanical forces in dextral rotation during cardiac looping in the chick embryo. Dev. Biol 2004;272:339–350. [PubMed: 15282152]
4. Ramasubramanian A, Latacha KS, Benjamin JM, Voronov DA, Ravi A, Taber LA. Computational model for early cardiac looping. Ann. Biomed. Eng 2006;34:1355–1369.
5. Nerurkar NL, Ramasubramanian A, Taber LA. Morphogenetic adaptation of the looping embryonic heart to altered mechanical loads. Dev. Dyn 2006;235:1822–1829. [PubMed: 16607653]
6. Hamburger V, Hamilton HL. A series of normal stages in the development of the chick embryo. J. Morphol 1951;88:49–92.
7. Voronov DA, Taber LA. Cardiac looping in experimental conditions: The effects of extraembryonic forces. Dev. Dyn 2002;224:413–421. [PubMed: 12203733]

8. Zamir EA, Srinivasan V, Perucchio R, Taber LA. Mechanical asymmetry in the embryonic chick heart during looping. Ann. Biomed. Eng 2003;31:1327–1336. [PubMed: 14758923]
9. Remond, MC. PhD thesis. St. Louis: Washington University; 2006. Mechanics of the Actomyosin Cytoskeleton during Looping of the Embryonic Chick Heart.
10. Zamir EA, Taber LA. Mechanical properties and residual stress in the stage 12 chick heart. J. Biomech. Eng 2004;126:823–830. [PubMed: 15796341]
11. Straight AF, Cheung A, Limouze J, Chen I, Westwood NJ, Sellers JR, Mitchison TJ. Dissecting temporal and spatial control of cytokinesis with a myosin II inhibitor. Science 2003;299:1743, 1747. [PubMed: 12637748]
12. Fujimoto JG. Optical coherence tomography for ultrahigh resolution in vivo imaging. Nat. Biotechnol 2003;21:1361, 1367. [PubMed: 14595364]
13. Jenkins MW, Rothenberg F, Roy D, Nikolski VP, Hu Z, Watanabe M, Wilson DL, Efimov IR, Rollins AM. 4d embryonic cardiography using gated optical coherence tomography. Optics Express 2006;23:736, 748.
14. Ramasubramanian A, Taber LA. Computational modeling of morphogenesis regulated by mechanical feedback. Biomech. Model. Mechanobiol. 2007(in press)
15. Rodriguez EK, Hoger A, McCulloch AD. Stress-dependent finite growth in soft elastic tissues. J. Biomech 1994;27:455, 467. [PubMed: 8188726]
16. Taber LA. Biomechanics of growth, remodeling, and morphogenesis. Appl. Mech. Rev 1995;48:487, 545.
17. Taber LA. Biomechanics of cardiovascular development. Annu. Rev. Biomed. Eng 2001;3:1–25. [PubMed: 11447055]
18. Taber, LA. Nonlinear Theory of Elasticity. Singapore: World Scientific; 2004.
19. Itasaki N, Nakamura H, Yasuda M. Changes in the arrangement of actin bundles during heart looping in the chick embryo. Anat Embryol 1989;180:413–420. [PubMed: 2619084]
20. Shiraishi I, Takamatsu T, Minamikawa T, Fujita S. 3-D observation of actin filaments during cardiac myofibrinogenesis in chick embryo using a confocal laser scanning microscope. Anat Embryol 1992;185:401–408. [PubMed: 1609966]
21. Filas BA, Efimov IR, Taber LA. Optical coherence tomography as a tool for measuring morphogenetic deformation of the looping heart. Anat. Rec 2007;290:1057–1068.
22. Taber LA. Biophysical mechanisms of cardiac looping. Int J. Dev. Biol 2006;50:323–332. [PubMed: 16479500]
23. Beloussov, LV. The Dynamic Architecture of a Developing Organism: An Interdisciplinary Approach to the Development of Organisms. the Netherlands: Kluwer, Dordrecht; 1998.
24. Holzapfel, GA. Nonlinear Solid Mechanics: A Continuum Approach for Engineering. John Wiley and Sons; 2001.
25. Harvey RP. Cardiac looping–an uneasy deal with laterality. Semin. Cell Dev. Biol 1998;9:101–108. [PubMed: 9572119]
26. Srivastava D, Olson EN. Knowing in your heart what' right. Trends Cell. Biol 1997;7:447–453. [PubMed: 17709004]
27. Mercola M, Levin M. Left-right asymmetry determination in the vertebrates. Ann Rev. Cell Dev. Biol 2001;17:779–805. [PubMed: 11687504]
28. Brand T. Heart development: Molecular insights into cardiac specification and early morphogenesis. Dev. Biol 2003;258:1–19. [PubMed: 12781678]
29. Okada Y, Nonaka S, Tanaka Y, Saijoh Y, Hamada H, Hirokawa N. Abnormal nodal flow precedes situs inversus in iv and inv mice. Mol. Cell 1999;4:459–468. [PubMed: 10549278]
30. Linask KK. Regulation of heart morphology: current molecular and cellular perspectives on the coordinated emergence of cardiac form and function. Birth Defects Res. (Part C) 2003;69:14–24.
31. Miller CE, Vanni MA, Taber LA, Keller BB. Passive stress-strain measurements in the stage-16 and stage-18 embryonic chick heart. J. Biomech. Eng 1997;119:445–451. [PubMed: 9407284]
32. Miller CE, Vanni MA, Keller BB. Characterization of passive embryonic myocardium by quasi-linear viscoelasticity theory. J. Biomech 1997;30:985–988. [PubMed: 9302625]

33. Miller CE, Wong CL. Trabeculated embryonic myocardium shows rapid stress relaxation and non-quasi-linear viscoelastic behavior. J. Biomech 2000;33:615–622. [PubMed: 10708783]

34. Ling P, Taber LA, Humphrey JD. Approach to quantify the mechanical behavior of the intact embryonic chick heart. Ann. Biomed. Eng 2002;30:636–645. [PubMed: 12108838]

35. Miller CE, Wong CL. Pressure overload alters stress-strain properties of the developing chick heart. Am. J. Physiol 2003;285:H1849–H1856.

36. Lacktis JW, Manasek FJ. An analysis of deformation during a normal morpho-genetic event. Birth Defects: Original Article Series 1978;14:205–227. [PubMed: 737298]

37. Zamir EA, Taber LA. On the effects of residual stress in microindentation tests of soft tissue structures. J. Biomech. Eng 2004;126:276–283. [PubMed: 15179859]

38. Taber LA. Theoretical study of Beloussov's hyper-restoration hypothesis for mechanical regulation of morphogenesis. Biomech. Modeling Mechanobiol. 2007(in press)

39. Linask KK, Han M, Cai DH, Brauer PR, Manisastry SM. Cardiac morphogenesis: Matrix metalloproteinase coordination of cellular mechanisms underlying heart tube formation and directionality of looping. Dev. Dyn 2005;233:739–753. [PubMed: 15844197]

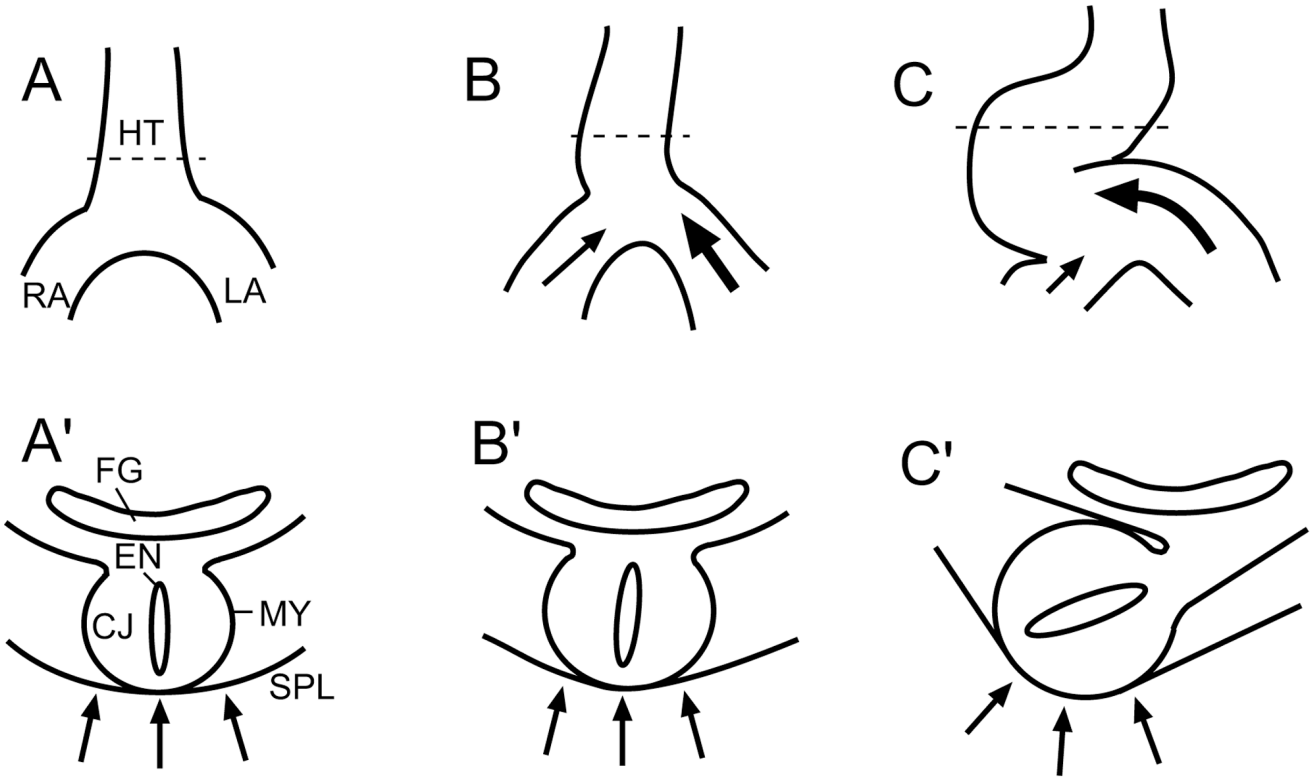

FIG. 1.

Schematic for cardiac rotation hypothesis. Ventral views (A,B,C) and cross-sectional views (A′,B′,C′) are shown, with locations of cross sections indicated by dashed lines in A,B,C. (HT = heart tube, LA = primitive left atrium, RA = primitive right atrium, CJ = cardiac jelly, MY = myocardium, EN = endocardium, SPL = splanchnopleure, FG = foregut) (A,A′) straight heart tube before looping. (B,B′) Both atria push against caudal end of the heart tube, and relatively greater force exerted by the left atrium displaces the heart tube slightly toward the right. (C,C′) The splanchnopleure pushes the heart tube dorsally, completing torsion.

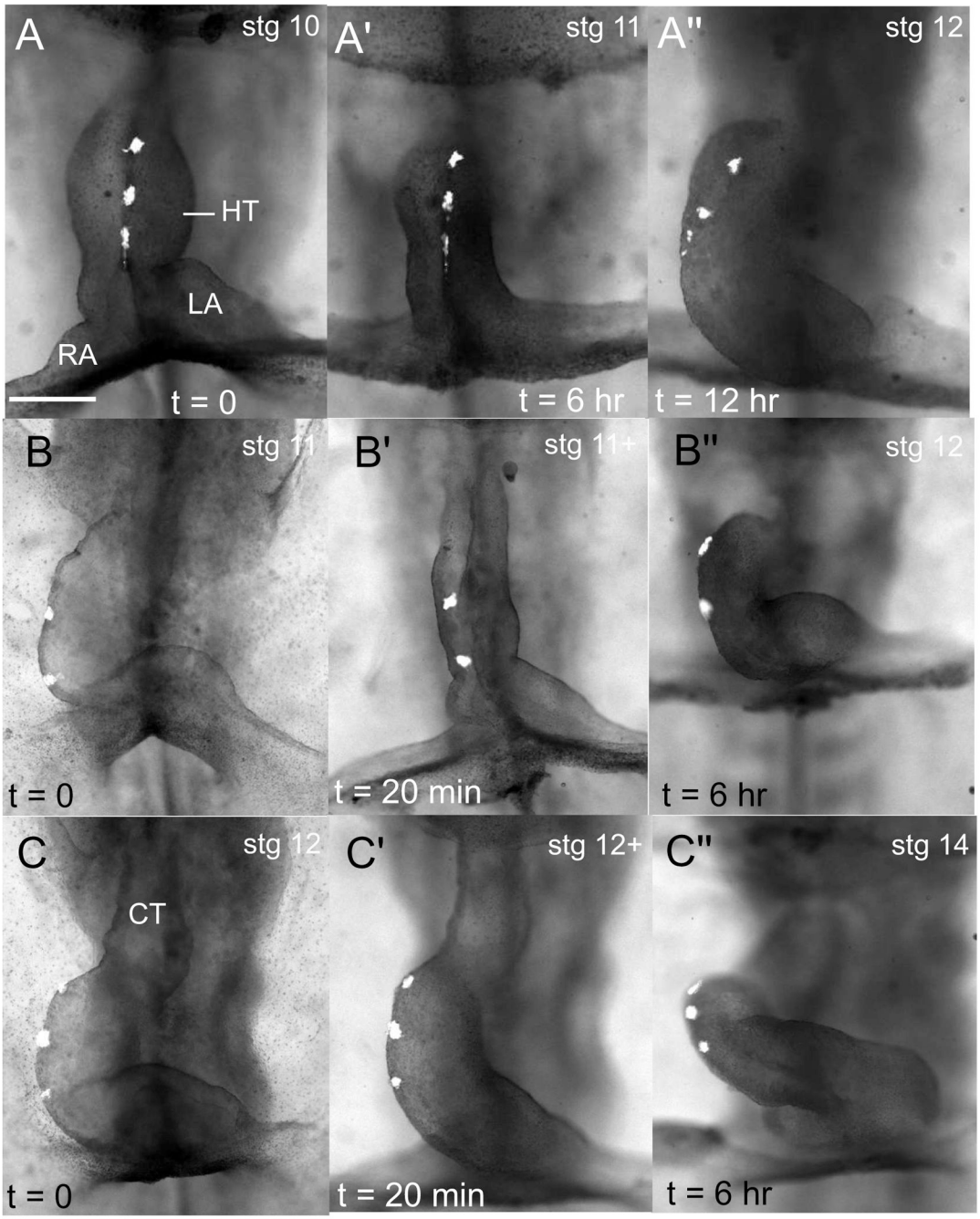

FIG. 2.

Effect of splanchnopleure (SPL) removal on cardiac torsion. Fluorescent labels are used to visualize rotation. SPL was removed at stage 10 (A–A″), stage 11 (B–B″), and stage 12 (A–A ″). (A) Stage 10 heart with SPL removed (HT=heart tube, RA=right atrium, LA=left atrium). (A″) Same heart after 6 hr culture (stage 11); little rotation occurred. (A″) Same heart after 12 hr culture (stage 12); rotation was fully restored. (B) Stage 11 heart with SPL intact. (B′) Same heart 20 min after SPL removal; heart partially untwisted, as shown by labels moving toward the center of HT. (B″) Same heart after 6 hr culture (stage 12); rotation was fully restored. (C) Stage 12 heart with SPL intact (CT = conotruncus). (C″) Same heart 20 min after SPL removal;

heart remained rotated. (C″) Same heart after 6 hr culture (stage 14); heart continued to develop normally. Scale bar = 200 μm

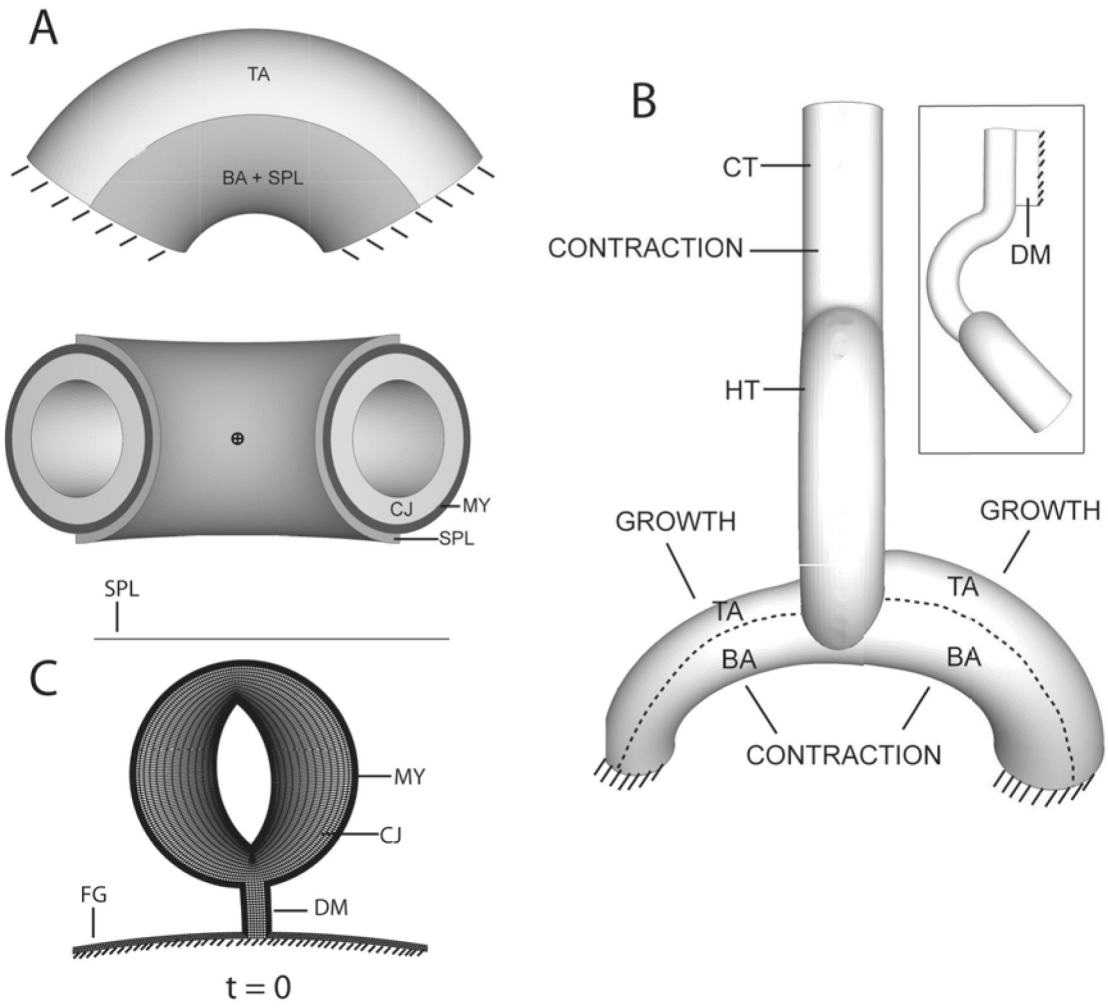

FIG. 3.

Finite element models (reference geometry). (A) Model for microindentation of primitive atria. Top: Ventral view; bottom: caudal view showing cross-section. Circle with cross hair denotes location of indenter. (B) Ventral view of 3-D model for looping heart (undeformed configuration) with loads and boundary conditions as indicated; insert shows side view. Note the angled atria and the fully bent heart tube. Dotted line in the atria denotes the longitudinal direction. (C) Two-dimensional (cross-sectional) model for cardiac rotation. (HT = heart tube, CT = conotruncus (outflow tract), TA = top atrial region, BA = bottom atrial region, DM = dorsal mesocardium, FG = foregut wall, MY = myocardium, CJ = cardiac jelly, SPL = splanchnopleure).

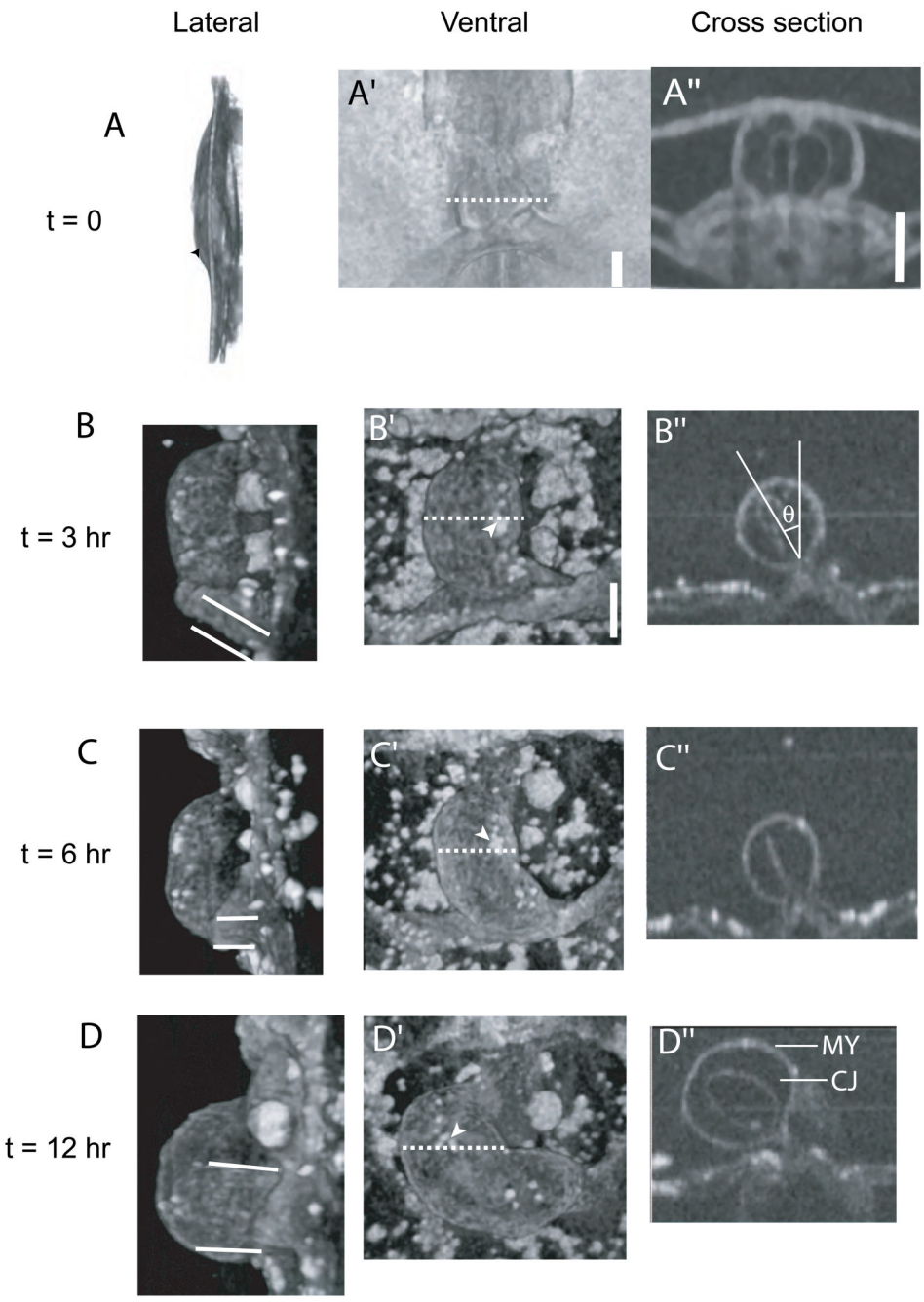

FIG. 4.

Optical coherence tomography (OCT) images of embryonic heart showing the effects of splanchnopleure (SPL) removal. (A–D) Left lateral view; (A′–D′) ventral view; (A″–D″) cross-sectional view of heart tube (HT) at locations indicated by dotted lines in ventral view. White arrowheads in B′–D′ mark the position of a cluster of beads used to visualize HT rotation; rotation angle θ is defined by orientation of lumen, as shown in (B″). (A–A″) Stage-10 heart with SPL intact. (B–B″) Heart with SPL removed after 3 hr culture. (C–C″) Same heart after 6 hr culture. Note that the bead cluster has not migrated rightward. (D–D″) Same heart after 12 hr culture. The bead cluster has migrated to the ventral midline, indicating rotation of heart. Rotation also can be seen in cross-sectional views (MY = myocardium, CJ = cardiac jelly).

Lines in (B)–(D) indicate orientation of primitive left atrium. Relative to the embryonic plane, the orientation angle progressively increases (approximately 30°, 45°, 90°, and 90° in A, B, C, and D, respectively.) Note: Panels B–B″, C–C″, and D–D″ are images of same heart. A different heart is used in (A)–(A″). Scale bars = 200 μm

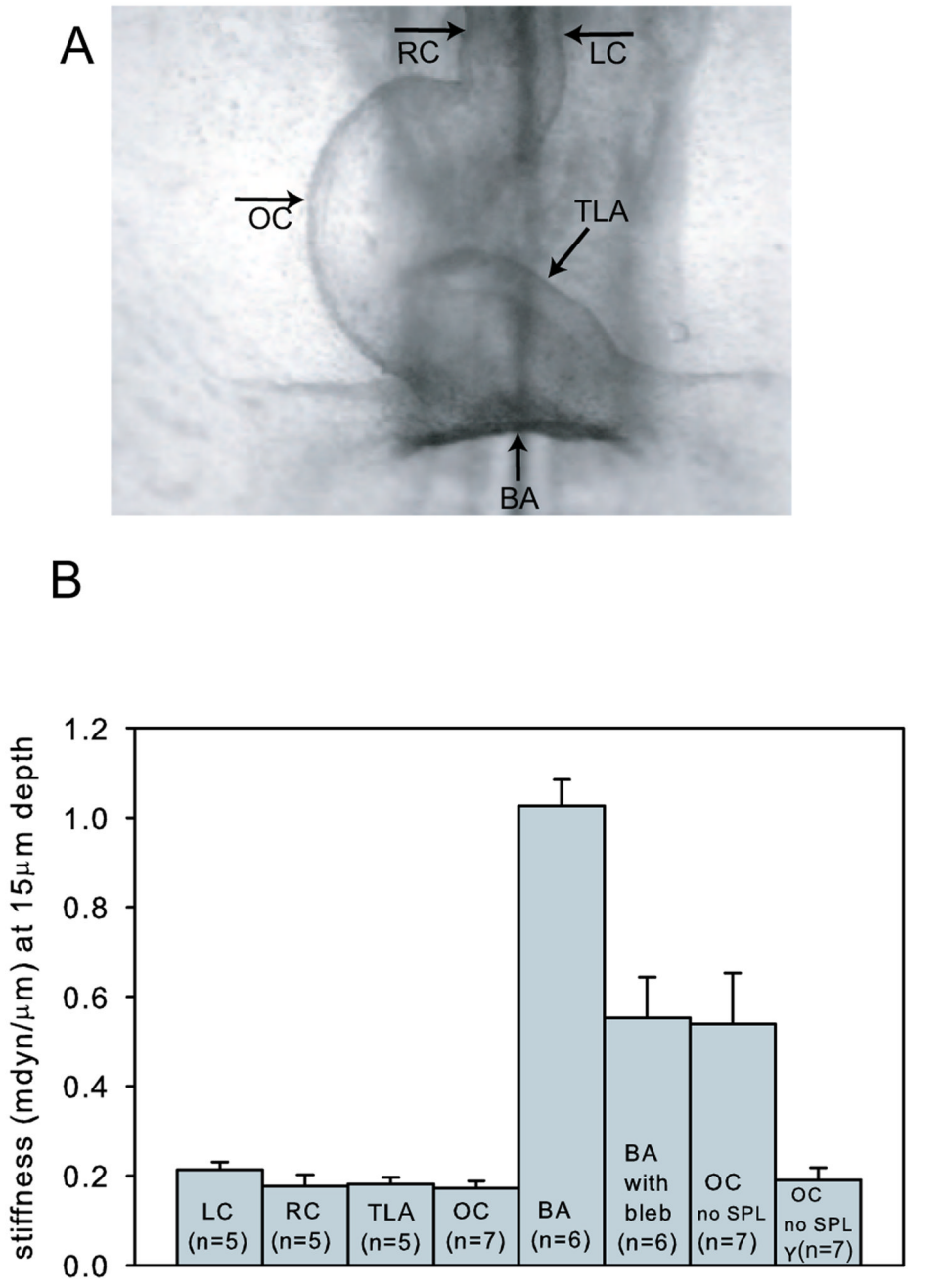

FIG. 5.

Stiffness measurements in normal stage-11 chick hearts. (A) Stage-11 heart indicating tested regions (LC = left side of conotruncus, RC = right side of conotruncus, TLA = top of left atrium, OC = outer curvature of heart tube), BA = bottom of atria. (B) Measured stiffness for each region at 15 μm indentation depth (mean ± SEM). For normal hearts (first five bars), region BA is significantly stiffer ($p < 0.001$) than the other regions, which have similar stiffnesses. (Data for normal OC are from [8].) Also shown are data for the following cases: BA exposed to 30 μM blebbistatin (bleb); OC of embryos cultured for 6 hr without splanchnopleure (no SPL; from [5]); OC of embryos cultured for 6 hr without splanchnopleure exposed to 12.5 μM

Y-27632 (no SPL, Y; from [5]). The cytoskeletal contraction inhibitors blebbistatin and Y-27632 significantly reduced stiffness ($p < 0.001$).

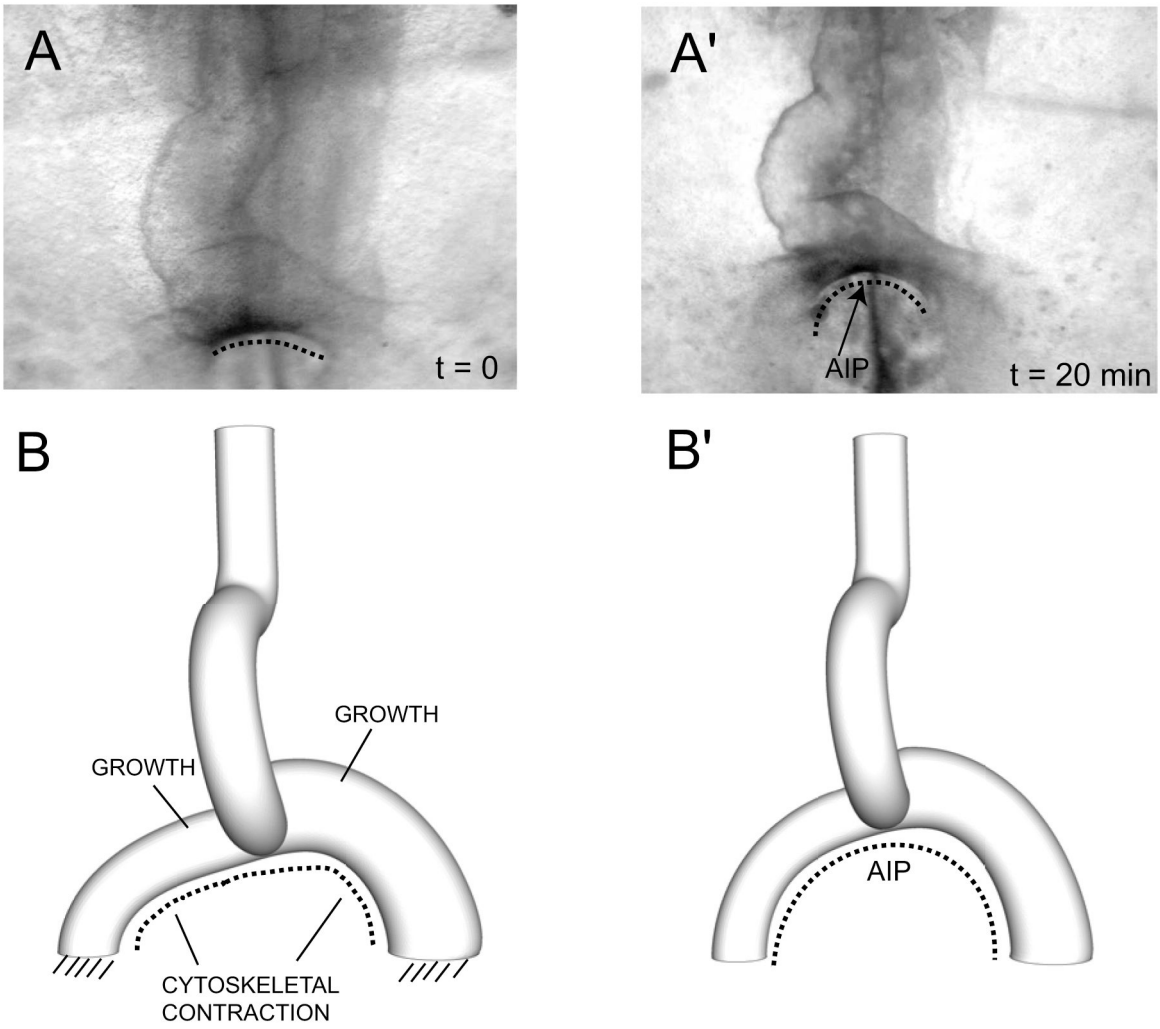

FIG. 6.

Effect of contraction on curvature of primitive atria. Dotted lines trace the shape of the anterior intestinal portal (AIP). (A) Normal heart at stage 10+; AIP curvature is relatively small. (A′) Same heart after 20 min exposure to 30 μM blebbistatin; AIP curvature increased dramatically. (B) Computational model of heart at stage 10+, with growth and contraction specified as indicated in atria. (B′) Same model with contraction turned off; curvature of the AIP increases as seen experimentally.

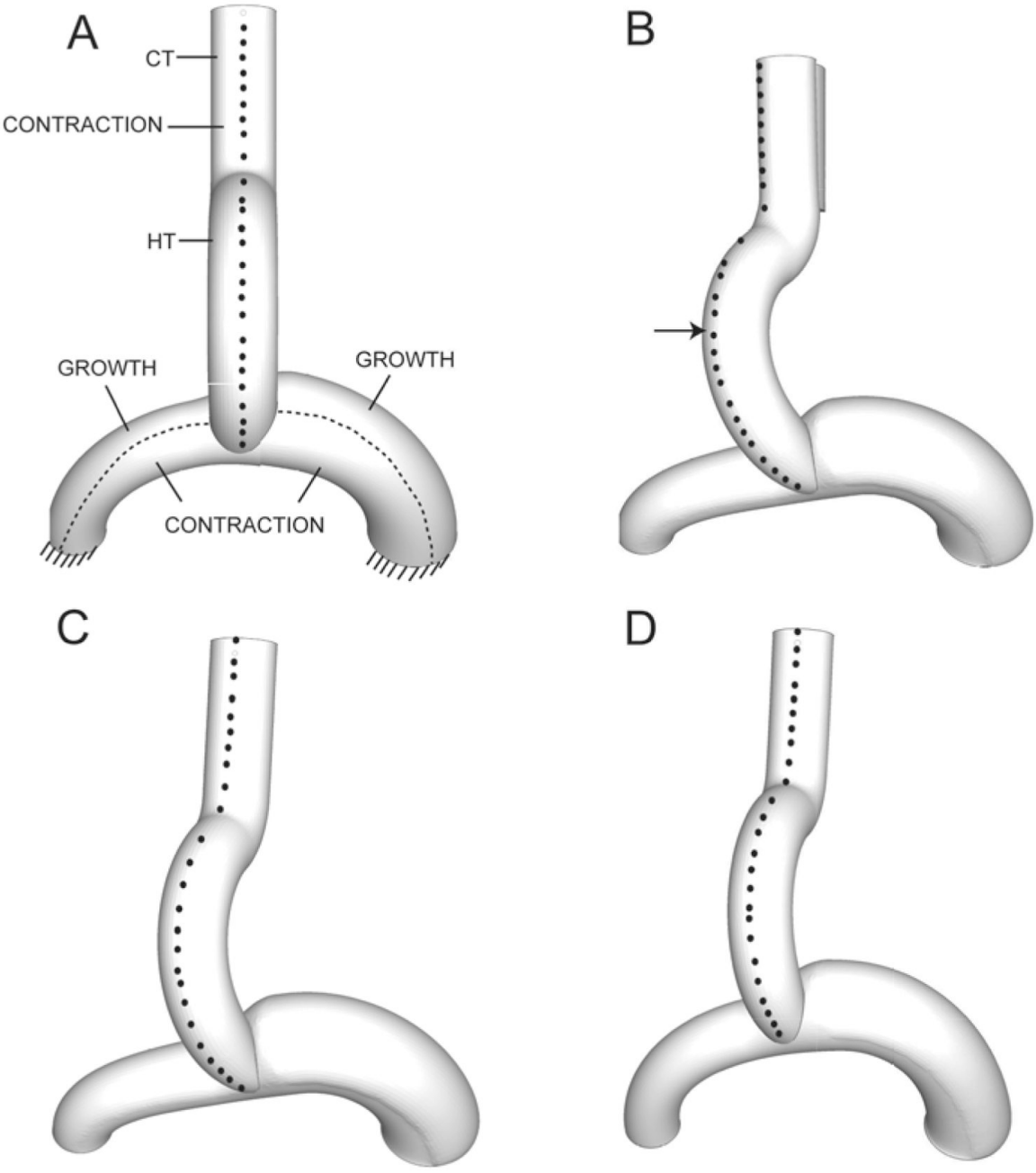

FIG. 7.

Three-dimensional finite element model for looping without splanchnopleure (ventral view). Nodes on the ventral midline are marked to visualize rotation: arrow in B marks the region where the rotation angle is measured (see schematic in Fig. 4B″) (HT = heart tube, CT = conotruncus). (A) Undeformed configuration with morphogenetic loads indicated. (B) Deformed configuration. Midline nodes move rightward as HT rotates, similar to experiment (see Fig. 2B″). (C) Same model with contraction turned off on right side of HT and CT; amount of rotation decreases. (D) Model with contraction turned off everywhere; rotation decreases further.

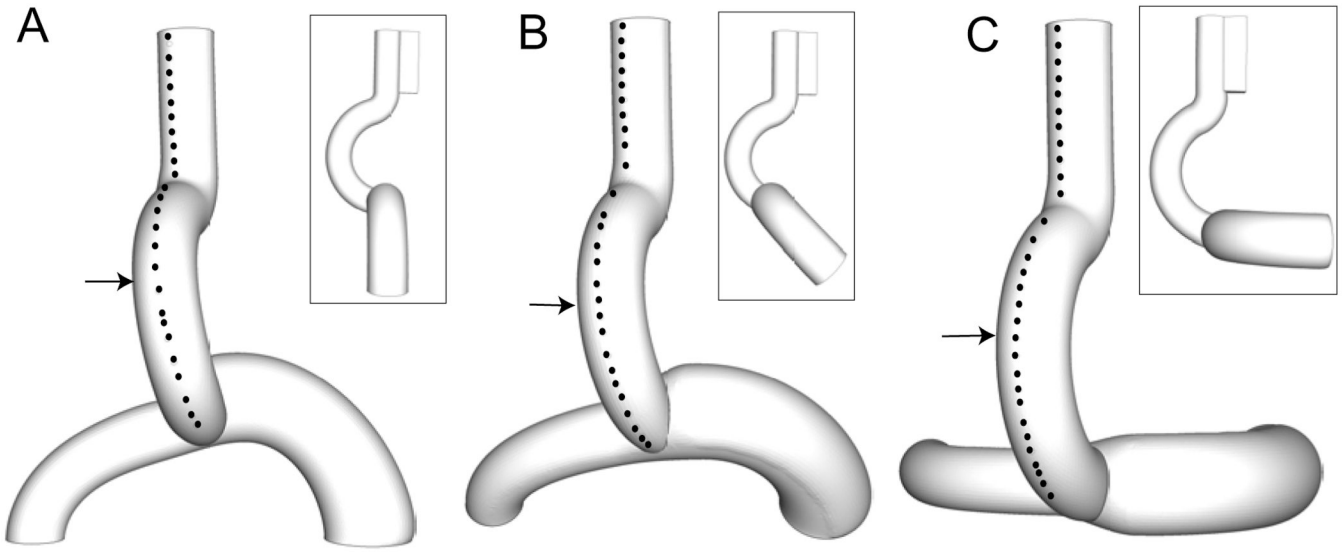

FIG. 8.

Effect of atria orientation on cardiac rotation. Arrows mark the regions where the lumen rotation angle is measured (see Fig. 4B″). Deformed ventral views are shown with inserts showing the undeformed side views. Filled circles mark midline nodes. (A) Atria lie in plane of embryo; rotation angle is 11°. (B) Atria are oriented 45° relative to embryonic plane; rotation angle is 24°. (C) Atria are oriented normal to embryonic plane; rotation angle is 24°.

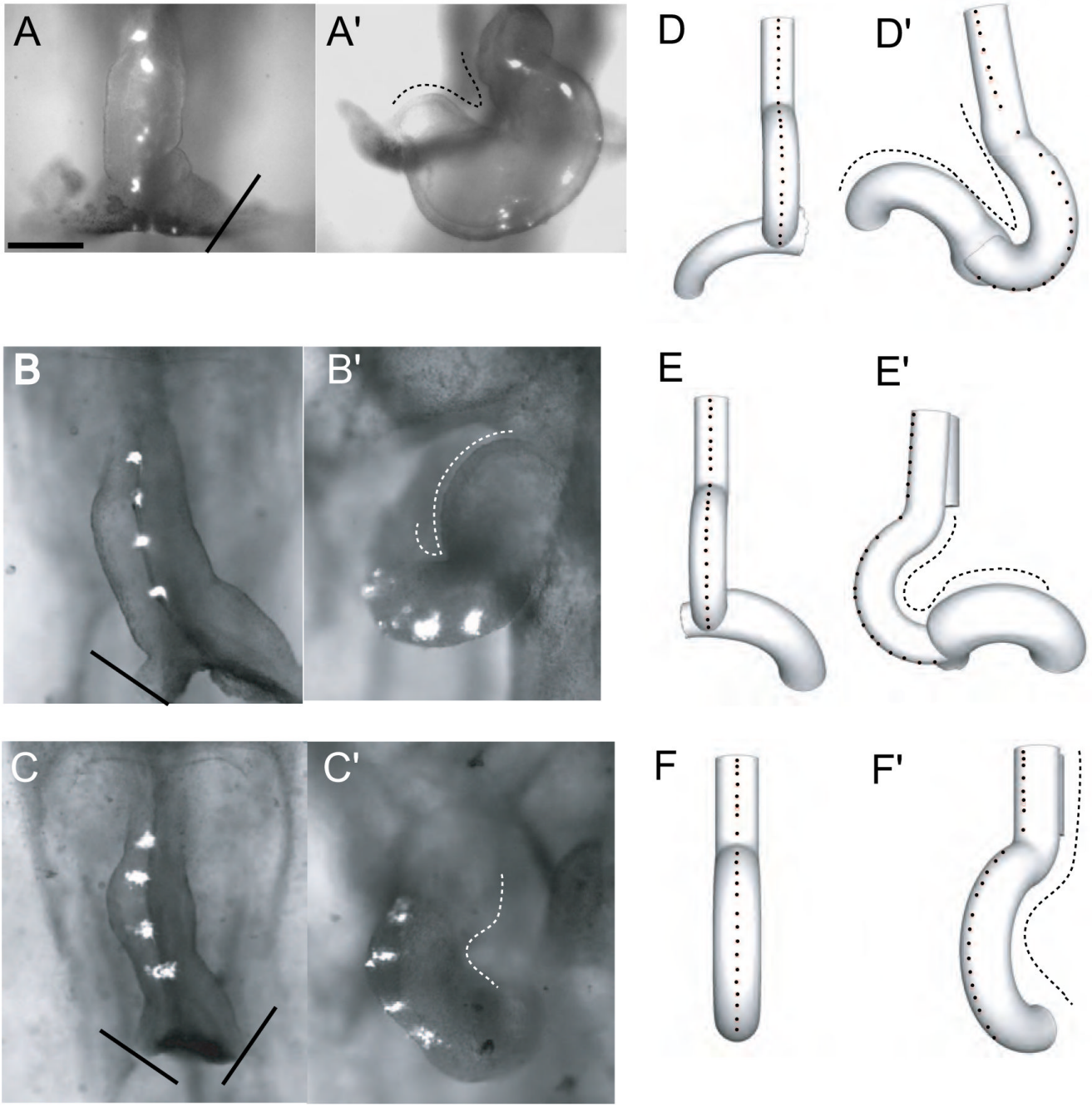

FIG. 9.

Experimental and computational effects of atria removal on looping. (A–C,D–F) Initial configuration (stage 10) with splanchnopleure (SPL) and at least one atrium removed (solid lines indicate cut locations). (A′–C′, D′–F′) Final configuration (approximately 12 hr later). Midline labels (experiment) and nodes (model) are used to visualize rotation. Top row: Left atrium is removed; heart loops leftward (11/15 in experiment). Middle row: Right atrium is removed; heart loops rightward with abnormal morphology (12/12 in experiment). Bottom row: Both atria are removed; rightward rotation occurs (14/14 in experiment). In each case, the model predicts approximately the correct heart shape, as indicated by dotted traces.

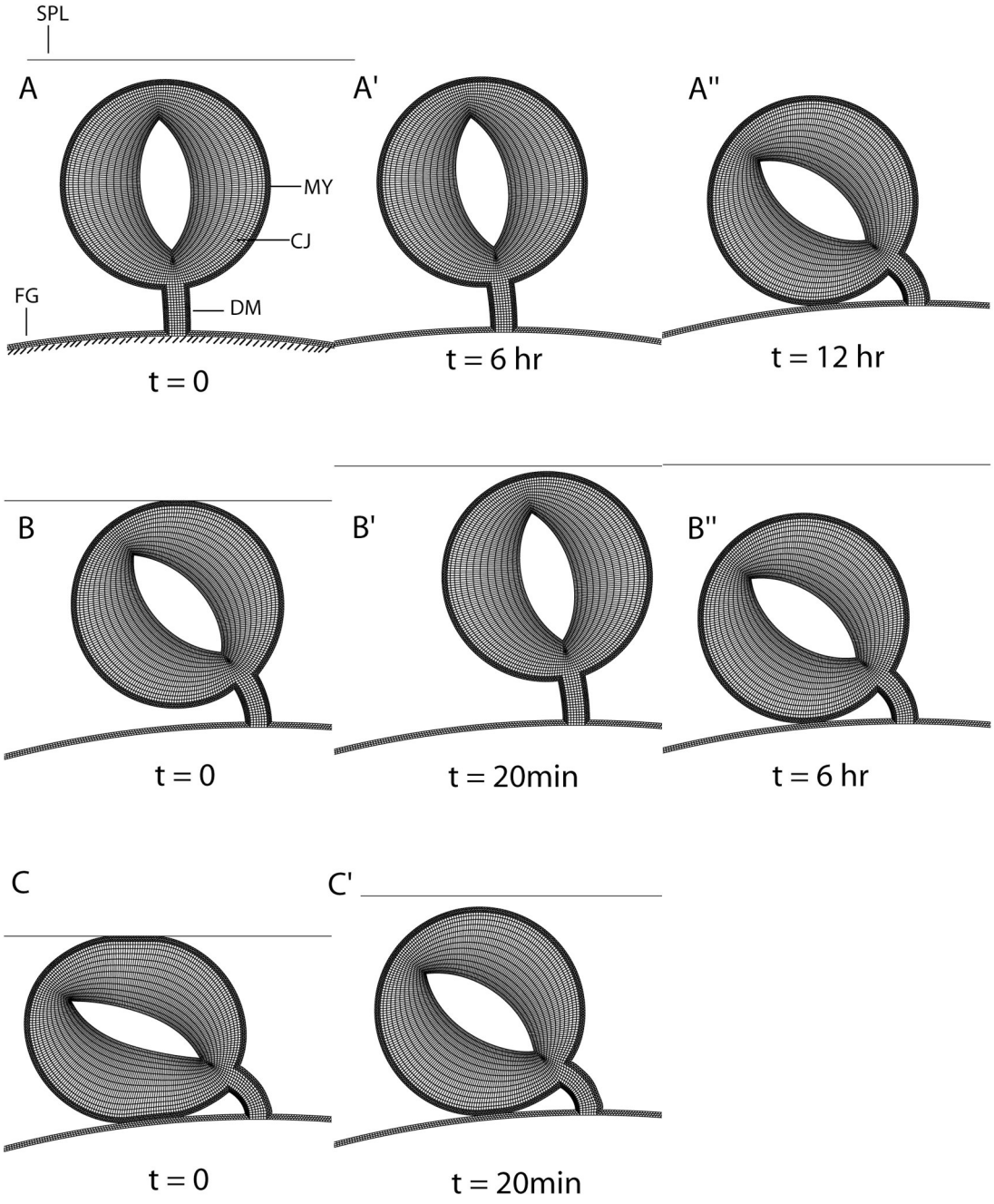

FIG. 10.

Two-dimensional model for cardiac rotation including mechanical feedback in the myocardium. Simulations show splanchnopleure (SPL) removal at stages 10 (A–A″), 11 (B–B″), and 12 (C–C″). Time $t = 0$ corresponds to these respective stages, and time points shown in each case correspond to the experimental time points shown in Fig. 2. (A) Model geometry for stage-10 heart (MY = myocardium, DM = dorsal mesocardium, CJ = cardiac jelly, FG = foregut wall). The heart is given a small initial rightward push, and then the load is removed. (A′) Little rotation occurs during the first six hours. (A″) After 12 hours, the heart has rotated fully. (B) Model for stage 11 heart with SPL in contact with the myocardium. (B′) When the SPL is removed, there is an immediate loss of rotation. (B″) Full rotation has occurred six hours

later. (C) Model for stage 12 heart with full rotation. (C′) Little rotation is lost when the SPL is removed.